Precision Engineering 55 (2019) 88–94

Contents lists available at ScienceDirect

Precision Engineering

journal homepage: www.elsevier.com/locate/precision

Energy-based friction analysis☆

Christoph Kossack, John Ziegert, Tony Schmitz*

Mechanical Engineering and Engineering Science, University of North Carolina at Charlotte, Charlotte, NC 28223, USA

ARTICLE INFO

Keywords:
Friction
Coulomb
Dynamics
Energy
Force

ABSTRACT

This paper describes a new approach for parameterizing friction models. Velocity measurements of a spring-mass-damper oscillator with a friction contact are used to determine the Coulomb friction coefficient for the friction-based energy dissipation. The energy-based friction force is then calculated and compared to the friction force determined from the product of the friction coefficient and normal force. The friction measuring machine, or FMM, is used to enable transient, linear sliding motion between friction contact pairs under constant normal force loading and a laser vibrometer is used to measure the corresponding time dependent velocity. Tests results are presented for a pin on oscillating flat contact with three different initial displacements. The measured velocity is used together with the FMM structural dynamics to determine the Coulomb friction coefficient and estimate the corresponding friction force during motion.

1. Introduction

The majority of friction measurements are made on tribometers, which apply a normal force to a pin (or other contact geometry) that is pressed against a rotating or reciprocating surface. Normal and friction forces are measured using single or multi-axis force dynamometers to parameterize the friction model. Primary uncertainty contributors for friction parameter estimation uncertainty using tribometers include:

- force transducer calibration
- cross-talk between the force axes for multi-axis dynamometers
- misalignment of the force measurement axes to the sliding direction and normal force application direction [1].

In this research, the traditional force-based (Newtonian) friction measurement paradigm is replaced by a velocity-based (Lagrangian) strategy. It is shown that velocity measurements can be used to parameterize a simple friction model and, subsequently, estimate friction force directly without the need for a force transducer. The friction measuring machine, or FMM, was used to enable transient, linear sliding motion between friction contact pairs under constant normal force loading [2,3]. FMM friction tests were completed for a pin on oscillating flat contact with three initial displacements. The initial displacement provided the input energy and the system oscillated until it came to rest (typically not at its starting position). The vibrometer measured the velocity during the decaying response as energy was dissipated in the friction contact (and FMM structure). The measured velocity was used together with the FMM structural dynamics to determine the friction coefficient and, by extension, the friction force during motion.

The paper is organized as follows. First, a background section is included. Second, a dynamic oscillator with sliding (Coulomb) friction is used to model the sliding contact and the associated second order differential equation of motion is defined [4]. Time domain solution of the equation of motion is then completed and an energy analysis is presented. Third, the flexure-based FMM is described [2,3]. Fourth, experimental results are presented where the Coulomb friction coefficient is determined by a fit to the decaying velocity signal and the corresponding friction force is calculated using the energy-based analysis. Fifth, conclusions are presented.

2. Background

Friction, which can be defined as the resistance to relative sliding between two bodies in contact under a normal load [5], is ubiquitous in manufacturing, metrology, mechanical design, and control. For manufacturing processes such as forging, rolling, extrusion, drawing, sheet metal forming, machining, and grinding, friction tends to increase the required force and power; therefore, the associated cost is significant. In forging, for example, friction forces at the die-workpiece interface can cause barreling, which yields inhomogeneous deformation patterns within the workpiece. It also leads to the familiar “friction hill” pressure

☆ This paper was recommended by Associate Editor Chinedum Okwudire.

* Corresponding author.
E-mail address: tony.schmitz@uncc.edu (T. Schmitz).

https://doi.org/10.1016/j.precisioneng.2018.08.011
Received 23 May 2018; Received in revised form 15 August 2018; Accepted 17 August 2018
Available online 01 September 2018
0141-6359/

distribution at the die-workpiece interface. In metal cutting, a high friction force is developed between the sheared chip and the rake face of the cutting tool in the secondary shear zone [5–9]. This, in turn, generates heat which tends to increase tool wear rates. For these and other reasons, the synthesis and testing of new lubricants and coatings to be used in manufacturing processes is an important, and continuous, research objective. Friction is also a necessary phenomenon, however. Without it, rolling, or reducing workpiece thickness using compressive forces applied by opposing rolls, would not be possible because the workpiece would not be pulled into the gap between the rolls.

Friction must also be considered in the control of manufacturing and metrology equipment. Servo-controlled, multi-axis positioning systems are widely used in: conventional and ultra-high precision machine tools; coordinate measuring machines; semi-conductor lithography equipment; micro- and nano-manufacturing systems; satellite imaging systems; and others. In many applications, axis positioning accuracies on the order of one part in 10^6 (or less) of the range of motion is required. For these high accuracy applications, motion velocities and accelerations are typically small, with the result that friction is often the dominant force in the system. This is true even when efforts are made to use very low friction interfaces, such as hydrostatic, aerostatic, or rolling contact bearings. Despite the use of tribological elements designed to reduce friction, it can still play a significant role in the system's positioning repeatability and accuracy [10].

Numerous strategies to account for and compensate frictional effects in position control systems have been reported [e.g, [10–14]]. However, implementation of model-based control is challenging because simple Coulomb-type friction models and many more advanced models, such as the Dahl, LuGre, Leuven, and generalized Maxwell-slip models, are discontinuous or piecewise continuous [15–24]. This poses a challenge for high performance continuous controllers (e.g., sliding mode control). Makkar et al. [25] presented a continuous and differentiable friction model which accounts for static and low-speed effects, position dependence, asymmetries, the Stribeck effect, and viscous damping. Other models are also available.

One common feature of these friction models is characterization of the frictional response near zero sliding speeds, where the “stiction” behavior transitions from no-slip to sliding motion. This is also the most critical region for high precision positioning controllers, particularly at motion reversals [26]. For example, cameras used for satellite imagery are positioned in low earth orbit at heights ranging from 300 km to 2000 km. In order for the camera to move its image point by 10 m on the earth's surface, the controller must be able to rotate the camera between 0.002 deg and 0.0003 deg, depending on the satellite height. Accurate realization of such motion is dependent on accurate characterization of the frictional behavior of the system near zero velocity.

Due to these considerations, modeling and measurement of friction behavior is a critical research topic for both engineering and the physical sciences. Friction models, such as those based on adhesion or other mechanisms, relate surface condition, normal load, sliding velocity, temperature, and environment, for example, to friction forces. Traditional friction measurement attempts to assign known operating conditions, while recording the resulting friction forces. In this way, friction models may be validated (or modified) and the performance of new lubricants and coatings may be assessed. In this research, this traditional force-based (Newtonian) friction measurement paradigm is replaced by a displacement-based (Lagrangian) strategy. In prior work, the measurement uncertainty for the force-based approach was evaluated and it was determined that its accuracy, particularly at low friction conditions, is limited [1]. The opportunity to reduce measurement uncertainty through the use of displacement-based (rather than force-based) metrology motivates the alternate Lagrangian measurement technique implemented here.

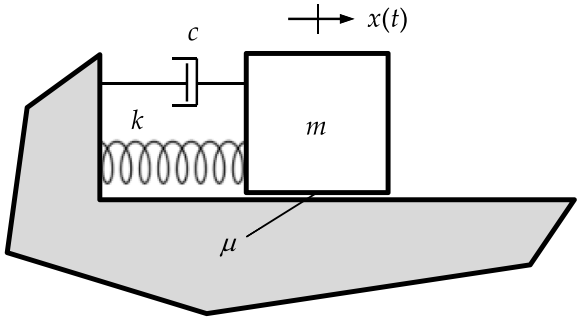

Fig. 1. Spring-mass-damper oscillator with Coulomb friction contact.

3. Sliding contact model

The dynamic oscillator displayed in Fig. 1 is used to model sliding friction. When the mass is given an initial displacement from its equilibrium position, this displacement characterizes the initial energy input to the system. The system is then released and allowed to oscillate until motion ceases. If the final rest position differs from the equilibrium position, potential energy remains in the system. During the decaying oscillation, the time dependent displacement and velocity describe the transient response. This characterizes the energy dissipation in a continuous time record. The dissipation describes the friction behavior at the interface over a range of sliding velocities from near-zero to the maximum.

Sliding, or Coulomb, friction is incorporated into the single degree of freedom, free vibration equation of motion that describes the time dependent displacement, $x(t)$, of Fig. 1 spring-mass system as shown in Eq. (1). In this equation, the time dependence is implied, m is the mass, c is the viscous dampener, k is the linear spring constant, and F_f is the friction force. For the Coulomb model, the friction force is equal to the product of the friction coefficient, μ, and the normal force, $N = mg$ (for Fig. 1 geometry).

$$\begin{aligned} m\ddot{x} + c\dot{x} + kx + F_f &= 0, \ \dot{x} > 0 \\ m\ddot{x} + c\dot{x} + kx &= 0, \ \dot{x} = 0 \\ m\ddot{x} + c\dot{x} + kx - F_f &= 0, \ \dot{x} < 0 \end{aligned} \tag{1}$$

Because the friction force always opposes the velocity direction, it is discontinuous. This yields the nonlinear second order, homogeneous differential equation shown in Eq. (1) [4]. For the velocity-based approach adopted in this research, the desired information is $\dot{x}(t)$, where the energy input is proportional to the square of the initial mass displacement, $x(0) = x_0$. Due to the friction force, the final displacement, x_f, depends on x_0.

To demonstrate, consider the case where $\mu = 0.24$, $m = 10.391$ kg, $c = 0.275$ N-s/m, and $k = 1982$ N/m for the model in Fig. 1. The free vibration response for $x_0 = 140$ mm (zero initial velocity) is displayed in Fig. 2, where $x_f = -9.297$ mm. It is observed that when the velocity reaches zero, if the current displacement is between $x_{lim} = \frac{F_f}{k} = \frac{\mu N}{k}$ and $-x_{lim}$, the motion stops. This limiting displacement (marked by the horizontal dashed lines in the top panel of Fig. 2) is the x value where the spring force is equal to or less than the maximum friction force. For a new initial displacement of $x_0 = 110$ mm, the final mass position is $x_f = 10.529$ mm; see Fig. 3. The results in Figs. 2 and 3 were obtained by fixed time step numerical integration of Eq. (1), where the acceleration is calculated at each time step and the corresponding velocity and displacement are determined by Euler integration [27]. The time step was selected to be 1×10^6 times smaller than the oscillating period for numerical accuracy.

Once the displacement and velocity are known, the kinetic and potential energy as a function of time can be calculated. The potential, PE, and kinetic, KE, energy expressions for the spring-mass-damper system are provided in Eqs. (2) and (3). Fig. 4 displays the time

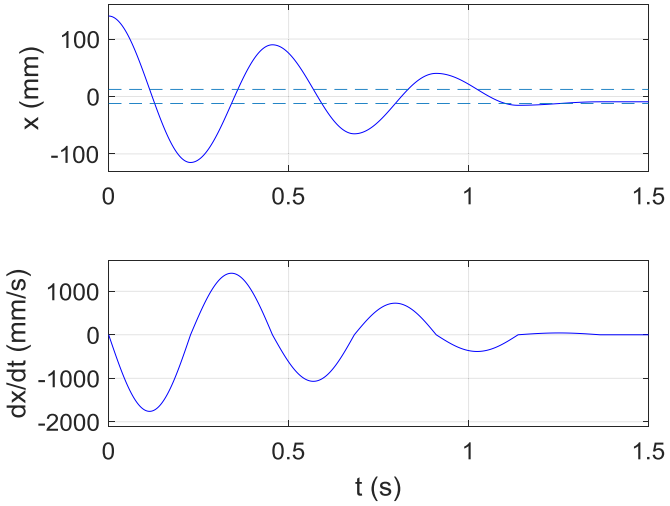

Fig. 2. Free vibration result for $x_0 = 140$ mm (zero initial velocity). (Top) Mass displacement versus time. (Bottom) Mass velocity versus time.

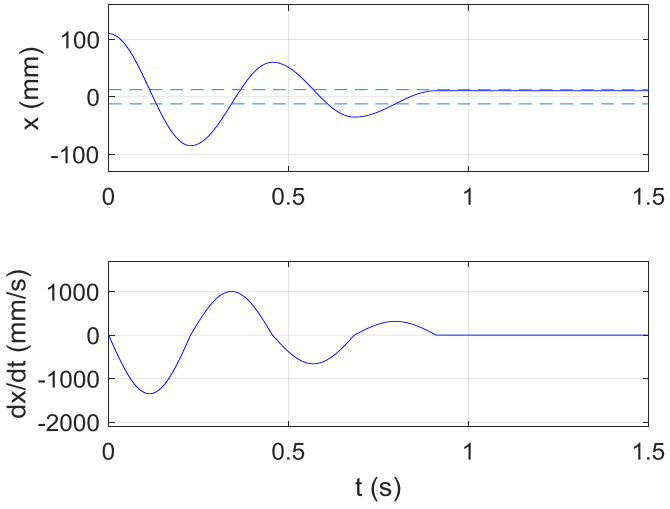

Fig. 3. Free vibration result for $x_0 = 110$ mm (zero initial velocity).

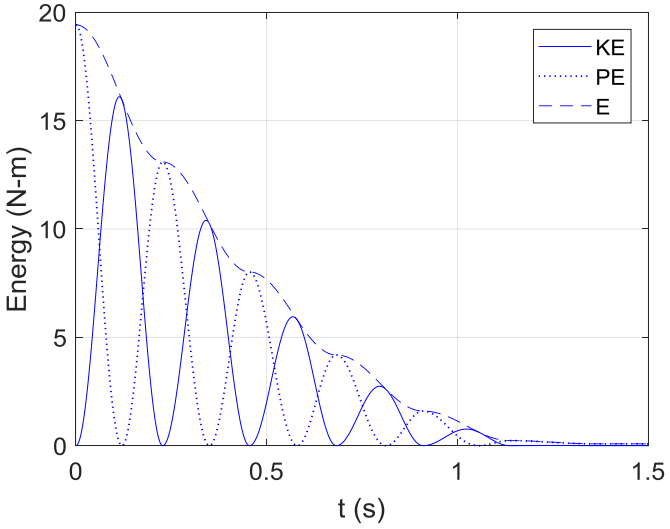

Fig. 4. Time dependent energy dissipation for $x_0 = 140$ mm (zero initial velocity).

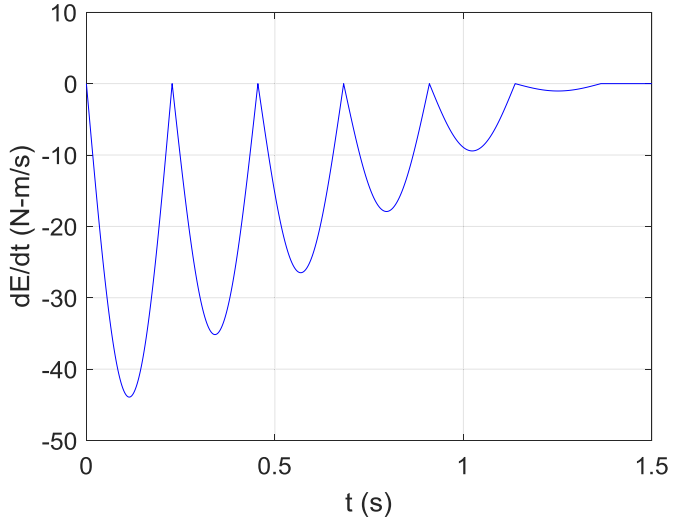

Fig. 5. Time dependent energy dissipation rate for $x_0 = 140$ mm (zero initial velocity).

dependent energy expressions, where $E = KE + PE$.

$$PE = \frac{1}{2}kx^2 \tag{2}$$

$$KE = \frac{1}{2}m\dot{x}^2 \tag{3}$$

The energy dissipation rate, $\dot{E}$, is the time derivative of E. It is calculated according to Eq. (4). Fig. 5 shows the variation in energy dissipation rate with time. The energy dissipation rate is momentarily zero when the system velocity goes to zero. Therefore, $\dot{E}$ is zero at each peak displacement and negative otherwise (because energy is being lost).

$$\dot{E} = \frac{d}{dt}\left(\frac{1}{2}kx^2 + \frac{1}{2}m\dot{x}^2\right) = m\dot{x}\ddot{x} + kx\dot{x} = \dot{x}(m\ddot{x} + kx) \tag{4}$$

The energy dissipation rate can be used to estimate the friction force by rewriting Eq. (4) and substituting this result in the oscillator equation of motion. First Eq. (4) is rewritten as shown in Eq. (5).

$$\frac{\dot{E}}{\dot{x}} = (m\ddot{x} + kx) \tag{5}$$

Second, the equation of motion is written as shown in Eq. (6).

$$m\ddot{x} + c\dot{x} + kx = (m\ddot{x} + kx) + c\dot{x} = F_f \tag{6}$$

Third, Eq. (5) is substituted in Eq. (6) to yield an expression for the friction force that is dependent on the energy dissipation rate and velocity. See Eq. (7). Because $\dot{E}$ depends on displacement and acceleration, the friction force solution requires knowledge of displacement, velocity, acceleration, and the oscillator single degree of freedom structural dynamics as represented by m, c, and k.

$$\frac{\dot{E}}{\dot{x}} + c\dot{x} = F_f \tag{7}$$

Fig. 6 displays the time dependent friction force during oscillator motion calculated using Eq. (7). The reference value (μN) is identified by the dashed line. The percent difference between the mean of Eq. (7) result and the reference value in Fig. 6 is 0.0025%. The difference occurs because the Euler integration scheme used to solve the equation of motion is non-conservative. However, the error is made negligibly small by decreasing the integration time step.

4. Experimental setup

The FMM provides relative linear motion between a friction contact

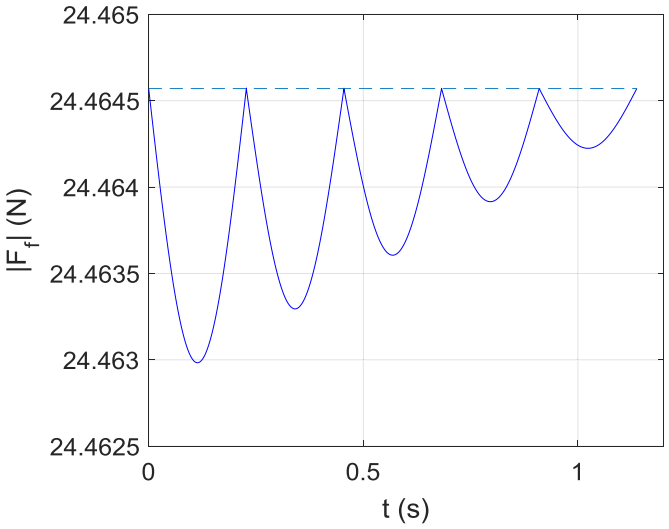

Fig. 6. Friction force calculated using Eq. (7) for $x_0 = 140$ mm (zero initial velocity).

pair (pin and flat counterface) using a parallelogram, leaf-type flexure. Fig. 7 displays the four leaf spring arrangement, where one end of each spring is clamped to a rigid base and the other is clamped to a faceplate which carries the motion platform. An electromagnet and linear actuator (not shown) are used to provide an initial displacement. A capacitance sensor (not shown) was used to monitor parasitic motion (i.e., arc motion perpendicular to the desired motion direction) of the platform. It was negligible when compared to the linear motion magnitude (e.g., 30 μm maximum parasitic motion for a 6 mm platform displacement).

The FMM dynamics with no friction contact were determined by: 1) imposing an initial displacement to the motion platform with the electromagnet and linear actuator (not shown in Fig. 7); 2) measuring the corresponding free vibration velocity after release; and 3) using a nonlinear least squares optimization function in MATLAB (*lsqnonlin*) to solve for the mass, damping, and spring constants that minimized the difference between the measured velocity and the solution to the damped oscillator's second order differential equation of motion, $m\ddot{x} + c\dot{x} + kx = 0$, where c is the viscous damping constant that was included to account for the small energy dissipation during the flexure motion. The results were: $m = 10.391$ kg, $c = 0.275$ N-s/m, and $k = 1982$ N/m. The corresponding undamped natural frequency and viscous damping ratio were: $f_n = \frac{1}{2\pi}\sqrt{\frac{1982}{10.391}} = 2.20$ Hz and $\zeta = \frac{c}{2\sqrt{km}} = \frac{0.275}{2\sqrt{1982(10.391)}} = 0.00096 = 0.096\%$. This low viscous damping ratio is typical for flexure-based motion platforms.

The FMM friction contact for FRF testing is produced between the pin and counterface. The 6.35 mm diameter pin is clamped into a holder with an extension of approximately 3 mm and then attached to the vertical shaft shown in Fig. 11. The shaft is supported by a pair of air bearings, which are rigidly attached to the base. The normal force between the pin and counterface is provided by a mass attached to the top of the vertical shaft. The mass for the tests completed in this study was 1.478 kg (normal force of 14.5 N).

After the pin is clamped to the vertical shaft, it is lowered onto sandpaper which is attached by adhesive tape to the counterface. The sample is then moved back and forth for several interations to ensure that the contacting surfaces are flat and parallel. This is repeated for a range of increasing grit numbers to leave a smooth pin face [1]. For the tests performed here, the contact pair consisted of a polytetrafluouroethylene (PTFE) pin on a polished steel counterface. The velocity was measured using a Polytec OFV-534 laser vibrometer head and OFV-5000 controller. The sampling frequency was 1000 Hz.

5. Results

The friction coefficient and corresponding friction force were estimated using the energy analysis for three different initial displacement values: {10, 14, and 22} mm. The data analysis procedure and experimental results are presented in the following paragraphs. Given the measured velocity and FMM structural dynamics, the simulation was used to determine a single best fit friction coefficient by comparing the measured and predicted velocity profiles for all three initial displacements. The fitting result for the 14 mm initial displacement is shown in Fig. 8 with a corresponding friction coefficient of 0.24. This approach differs significantly from the traditional pin-on-disk force-based approach, where the normal and friction components are measured directly and their ratio is used to determine the friction coefficient for a fixed sliding speed. Here, the time dependent velocity is used to parameterize the simple friction model.

The displacement and acceleration were determined by numerical integration and differentiation, respectively, of the measured velocity. Because differentiation tends to amplify noise, a moving average filter with a span of 10 points was applied to the acceleration signal. The results are presented in Figs. 9 and 10. For reference, the simulated

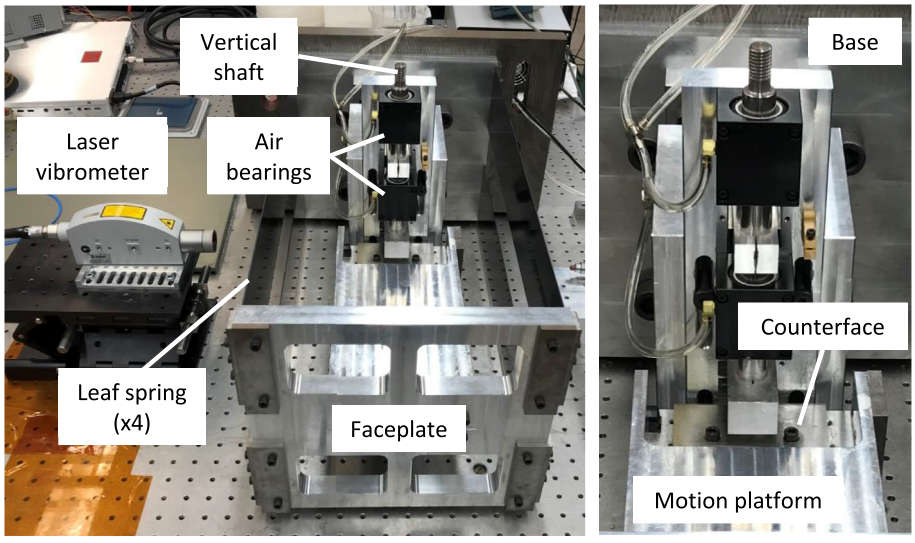

Fig. 7. Photograph of FMM. The key components are identified.

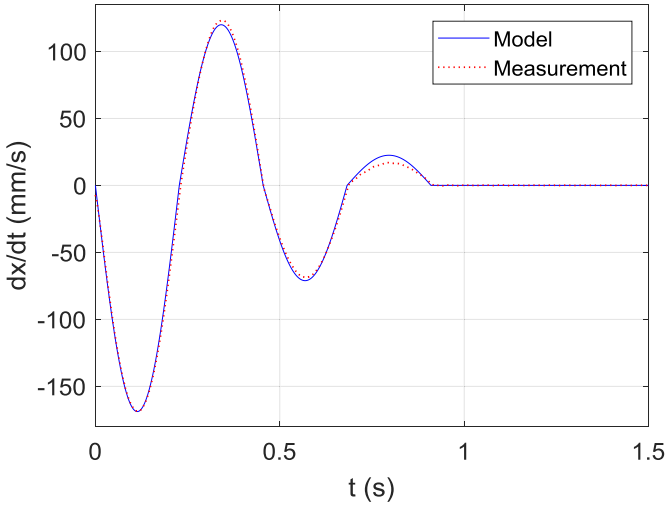

Fig. 8. Fitting result for the time domain velocity for $x_0 = 14$ mm (zero initial velocity).

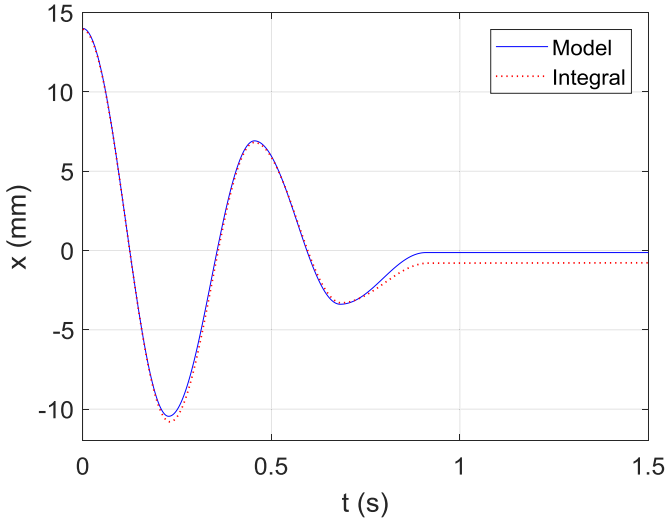

Fig. 9. Integration of measured velocity to obtain displacement for $x_0 = 14$ mm (zero initial velocity).

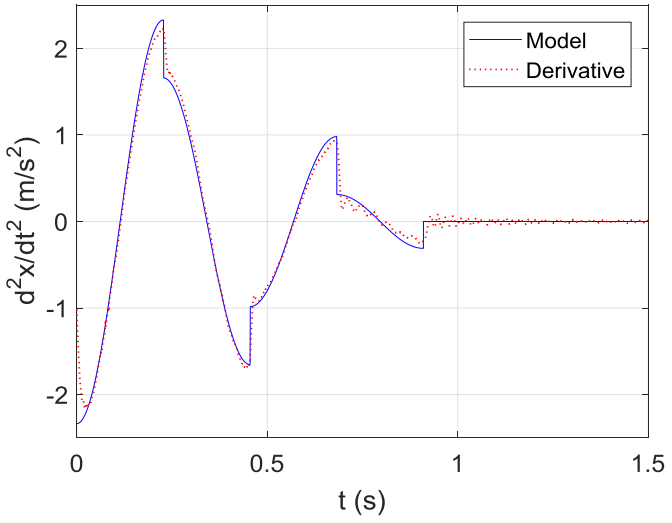

Fig. 10. Differentiation of measured velocity to obtain acceleration for $x_0 = 14$ mm (zero initial velocity).

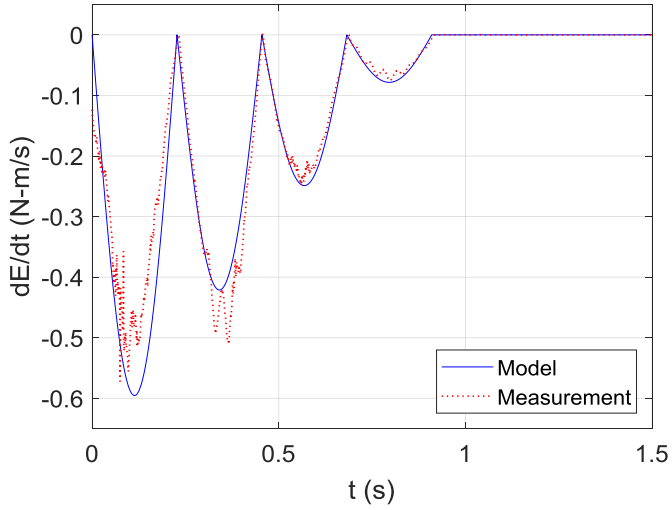

Fig. 11. Time dependent energy dissipation rate for $x_0 = 14$ mm (zero initial velocity).

signals are included as well, although they are not required to carry out the friction force calculation by Eq. (7).

Using the displacement, velocity, acceleration, friction coefficient, and structural dynamics, the energy dissipation rate analysis was completed. The energy dissipation rate is presented in Fig. 11; it was calculated using Eq. (4). The corresponding friction force is displayed in Fig. 12 for the oscillating time interval (Eq. (7)). The reference value (μN) is also included (dashed line). Although there is significant noise in the predicted force, the mean value agrees with the reference value to 1.9%.

The analysis was repeated for initial displacements of 10 mm and 22 mm. The 10 mm velocity fit is shown in Fig. 13 and the friction force is shown in Fig. 14. The percent difference between the predicted mean and reference value is 8.0%.

The 22 mm velocity fit is shown in Fig. 15 and the friction force is shown in Fig. 16. The percent difference between the predicted mean and reference value is −4.3%.

In order to parameterize friction models with low uncertainty using the Lagrangian approach presented here, the displacement metrology and modal parameters that describe the FMM structural dynamics must also have low uncertainty; see Eqs. (1) and (7). The use of separate

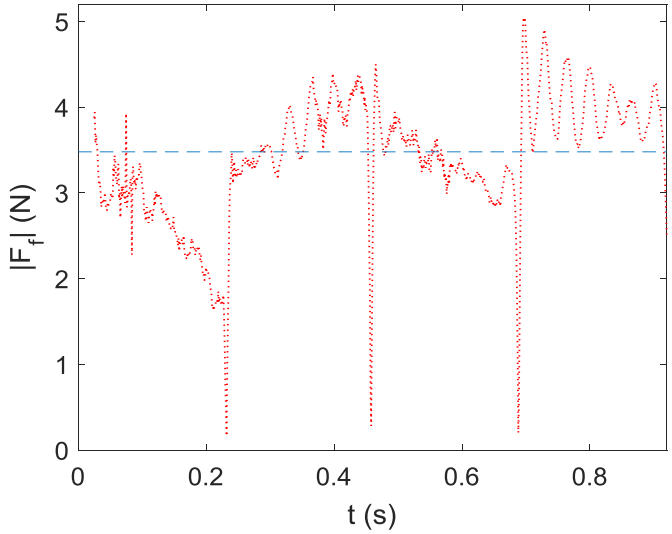

Fig. 12. Absolute value of the friction force predicted by Eq. (7) analysis for $x_0 = 14$ mm (zero initial velocity).

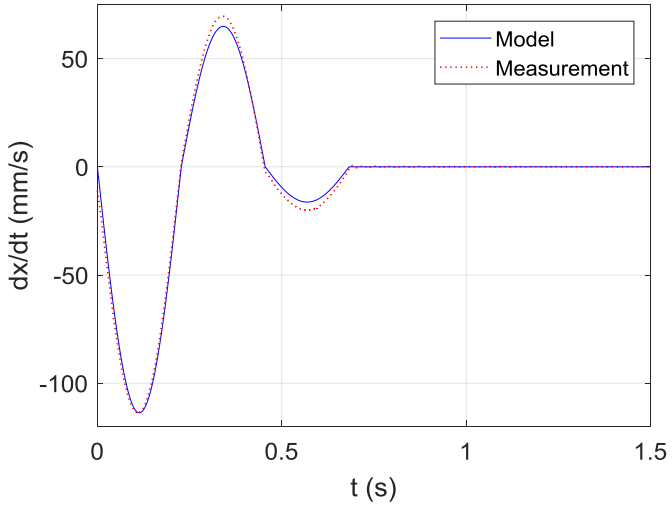

Fig. 13. Fitting result for the time domain velocity for $x_0 = 10$ mm (zero initial velocity).

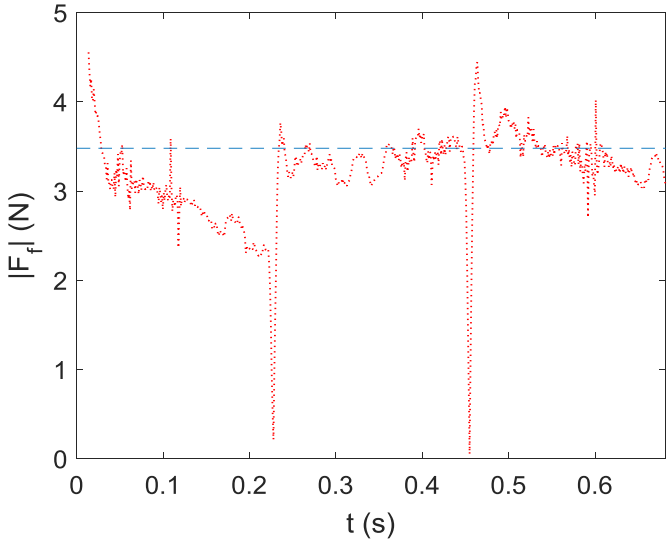

Fig. 14. Absolute value of the friction force predicted by Eq. (7) analysis for $x_0 = 10$ mm (zero initial velocity).

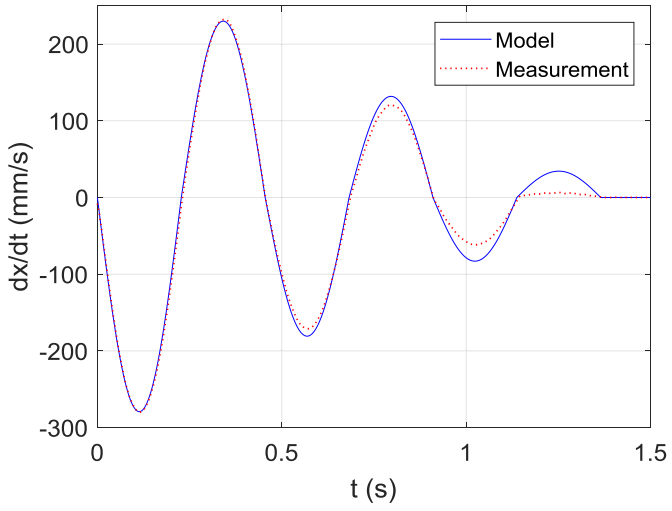

Fig. 15. Fitting result for the time domain velocity for $x_0 = 22$ mm (zero initial velocity).

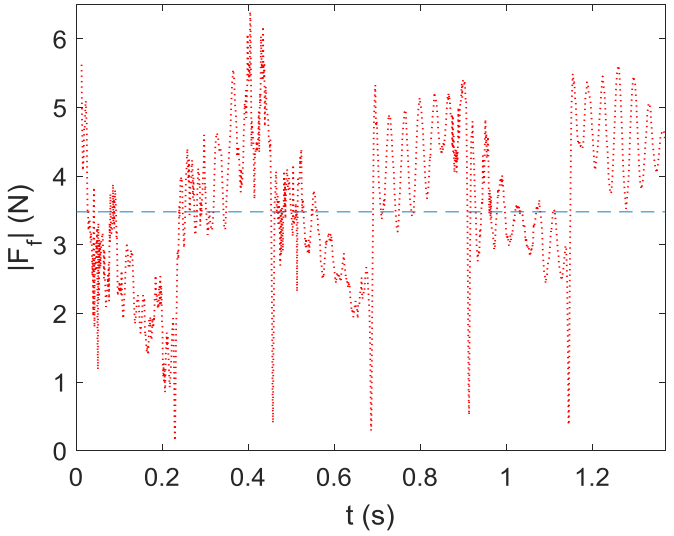

Fig. 16. Absolute value of the friction force predicted by Eq. (7) analysis for $x_0 = 22$ mm (zero initial velocity).

sensors for displacement (displacement measuring interferometer), velocity (laser vibrometer), and acceleration (piezoelectric accelerometer) should enable the required measurement uncertainty levels to be obtained. For the modal parameters, these can be determined from separate free vibration tests (no friction contact). A related FMM study identified the mean modal mass value to be 10.391 kg with a standard deviation of 0.0049 kg (0.047%) over a range of initial displacements from 4 mm to 22 mm. The corresponding modal stiffness was 1982 N/m with a standard deviation of 1.3 N/m (0.066%) [28].

6. Conclusions

This paper presents an alternative approach to parameterize friction models using measured velocity from an oscillating friction contact. This characterization of frictional behavior that does not rely on the traditional measurement of forces, but instead tracks the rate of energy dissipation in an oscillating system. The energy-based analysis also provides a way to estimate the friction force. While the theoretical derivation provides an expression for computing the friction force directly from the measured oscillator motion (Eq. (7)), in practice the digital differentiation of the velocity signal to obtain acceleration introduces significant noise into the result. An advantage of this approach is that it enables the evaluation of any friction model, including those that exhibit velocity dependence and Stribeck friction behavior near zero velocity, for example. The use of an oscillating dynamic system ensures that the system will reach zero velocity multiple times during the test and, therefore, offers a new approach to characterizing frictional behavior over a range of sliding velocities. Future work includes evaluation of this approach for lubricated and rolling contacts, as well as the addition of accelerometers to directly measure system acceleration instead of digitally differentiating the velocity signal.

Acknowledgements

The authors acknowledge the contributions of C. Lomascolo to the FMM construction.

References

[1] Schmitz T, Action J, Ziegert J, Sawyer WG. The difficulty of measuring low friction: Uncertainty analysis for friction coefficient measurements. J Tribol 2005;127:673–8.
[2] Lomascolo C, Ziegert J, Schmitz T. Displacement-based measurement of static and dynamic coefficients of friction. American society for precision engineering annual

meeting, october 23-28, Portland, OR. 2016.
[3] Kossack C, Schmitz T, Ziegert J. Identification of friction energy dissipation using free vibration velocity: Measurement and modeling. American society for precision engineering annual meeting, october 29-November 3, Charlotte, NC. 2017.
[4] Inman DJ. Engineering vibration vol. 3. New Jersey: Prentice Hall; 2008.
[5] Kalpakjian S, Schmid S. Manufacturing processes for engineering materials. fifth ed. Upper Saddle River, NJ: Prentice Hall; 2008.
[6] Astakhov V. Tribology of metal cutting. Oxford, UK: Elsevier Science and Technology; 2006.
[7] Astakhov V. Metal cutting mechanics. Boca Raton, FL: CRC Press; 1998.
[8] Tlusty G. Manufacturing processes and equipment. Upper Saddle River, NJ: Prentice Hall; 1999.
[9] Yang X, Liu CR. A new stress-based model of friction behavior in machining and its significant impact on residual stresses computed by finite element method. Int J Mech Sci 2002;44:703–23.
[10] Olsson H, Åström KJ, Canudas de Wit C, Gäfvert M, Lischinsky P. Friction models and friction compensation. Eur J Contr 1998;4/3:176–95.
[11] Armstrong-Helouvry B. Control of machines with friction. Boston, MA: Kluwer; 1991.
[12] Armstrong-Helouvry B, Dupont P, Canudas de Wit C. A survey of models, analysis tools and compensation methods for the control of machines with friction. Automatica 1994;30/7:1083–138.
[13] Berger EJ. Friction modeling for dynamic system simulation. Appl Mech Rev 2002;55/6:535–77.
[14] Hsu S, Ying C, Fei Z. The nature of friction: a critical assessment. Friction 2014;2/1:1–26.
[15] Barahanov N, Ortega R. Necessary and sufficient conditions for passivity of the LuGre friction model. IEEE Trans Automat Contr 2000;45/4:830–2.
[16] Bliman PA, Sorine M. Easy-to-use realistic dry friction models for automatic control. Proceedings of the 3rd European control conference, ECC'95, Rome, Italy. 1995. p. 3788–94.
[17] Canudas de Wit C, Olsson H, Astrom KJ, Lischinsky P. A new model for control of systems with friction. IEEE Trans Automat Contr 1995;40:419–25.
[18] Dahl P. A solid friction model El Segundo, CA: The Aerospace Corporation; 1968. Tech. Rep. TOR-0158(3107-18).
[19] Dupont P, Hayward V, Armstrong B, Altpeter F. Single state elastoplastic friction models. IEEE Trans Automat Contr 2002;47:683–7.
[20] Ferretti G, Magnani G, Martucci G, Rocco P, Stampacchia V. Siciliano B, Dario P, editors. Friction model validation in sliding and presliding regimes with high resolution encoders, Experimental Robotics VIII. New York: Springer-Verlag; 2003. p. 328–37.
[21] Ferretti G, Magnani G, Rocco P. Single and multistate integral friction models. IEEE Trans Automat Contr 2004;49:2292–7.
[22] Lampaert V, Swevers J, Al-Bender F. Modification of the Leuven integrated friction model structure. IEEE Trans Automat Contr 2002;47/4:683–7.
[23] Swevers J, Al-Bender F, Ganseman CG, Prajogo T. An integrated friction model structure with improved presliding behavior for accurate friction compensation. IEEE Trans Automat Contr 2000;45:675–86.
[24] Lampaert V, Al-Bender F, Swevers J. A generalized Maxwell-slip friction model appropriate for control purposes. IEEE international conference on physics and control proceedings-physcon, st. Petersburg, Russia. 2003. p. 24–31.
[25] Makkar C, Dixon W, Sawyer WG, Hu G. A new continuously differentiable friction model for control systems design. Proceedings of the 2005 IEEE/ASME international conference on advanced intelligent mechatronics, monterey, CA, July 24-28. 2005. p. 600–5.
[26] Jamaludin Z, Brussel HV, Pipeleers G, Swevers J. Accurate motion control of XY high-speed linear drives using friction model feedforward and cutting forces estimation. CIRP Ann - Manuf Technol 2008;57/1:403–6.
[27] Schmitz T, Smith KS. Mechanical vibrations: Modeling and measurement. New York, NY: Springer; 2012.
[28] Kossack C. Friction measurement during free vibration. Charlotte, NC: MS Thesis, UNC Charlotte; 2018.